Published in final edited form as:
Dev Cell. 2009 December ; 17(6): 823–835. doi:10.1016/j.devcel.2009.10.022.

Dual Modes of Cdc42 Recycling Fine-Tune Polarized Morphogenesis

Brian D. Slaughter[1], **Arupratan Das**[1], **Joel W. Schwartz**[1,2], **Boris Rubinstein**[1,4], and **Rong Li**[1,3,4]

[1] Stowers Institute for Medical Research 1000 East 50th Street Kansas City, MO 64110

[3] Department of Molecular and Integrative Physiology University of Kansas Medical Center 3901 Rainbow Boulevard Kansas City, Ks 66160

Summary

In budding yeast, the highly-conserved small GTPase Cdc42 localizes to the cortex at a cell pole and orchestrates the trafficking and deposition of cell surface materials required for building a bud or mating projection (shmoo). Using a combination of quantitative imaging and mathematical modeling, we elucidate mechanisms of dynamic recycling of Cdc42 that balance diffusion. Rdi1, a guanine nucleotide dissociation inhibitor (GDI), mediates a fast recycling pathway, while actin patch-mediated endocytosis accounts for a slower one. These recycling mechanisms are restricted to the same region of the nascent bud, as both are coupled to the Cdc42 GTPase cycle. We find that a single dynamic parameter, the rate of internalization inside the window of polarized delivery, is tuned to give rise to distinct shapes of Cdc42 distributions that correlate with distinct morphogenetic fates, such as the formation of a round bud or a pointed shmoo.

Introduction

Polarized morphogenesis refers to the processes that give rise to distinct asymmetric cell shapes such as those of a neuron, epithelial cell, and filamentous fungus, etc, which are critical for specialized functions and physiology of these cells and organisms. The establishment of cell polarity, which results in the localization of signaling and cytoskeletal components that subsequently organize the growth of distinct cell structures, is a key step in polarized morphogenesis. While recent studies have led to considerable insights into the initial symmetry breaking processes that establish cell polarity (Li and Gundersen, 2008; Onsum and Rao, 2009), it remains poorly understood how polarized distributions of key regulatory molecules are stably maintained and are fine-tuned to give rise to different morphogenetic outcomes in response to diverse physiological or developmental signals.

A key regulator of cell polarity in many eukaryotes is the Rho-family GTPase Cdc42 (Etienne-Manneville, 2004), first discovered in the yeast *Saccharomyces cerevisiae* (Johnson, 1999).

4 To whom correspondence should be addressed. rli@stowers.org ph. 816.926.4340, fax 816.926.4660 bru@stowers.org ph. 816.926.4403, fax 816.926.4674.
[2]Current address: Department of Neurobiology Duke University Medical Center Box 3209 Bryan Research Building, Research Drive Durham, NC 27710

G1 phase yeast cells polarize to initiate bud formation or in response to pheromone to form the mating projection (shmoo). During both these processes, Cdc42 localizes to a small cortical domain, which becomes the presumptive bud or shmoo site (Richman et al., 2002; Ziman et al., 1993). The localized Cdc42 orchestrates the morphological development of a bud or shmoo by controlling the formation of oriented actin cables that direct transport of membrane vesicles and organelles, the assembly of a ring of septins that define the bud neck, and the specification of the site of exocytic vesicle fusion (Park and Bi, 2007; Wedlich-Soldner and Li, 2004). Cdc42 cycles between two guanine nucleotide (GTP and GDP)-bound states. This cycle is controlled by Cdc42's guanine nucleotide exchange factor (GEF), Cdc24, and several GTPase activating proteins (GAPs) (Park and Bi, 2007). In its GTP bound form, Cdc42 interacts with a wide range of effectors that control downstream functions (Park and Bi, 2007). Effector interactions and the assembly of a polarized actin cytoskeleton also constitute feedback loops that enhance the accumulation of active Cdc42 during the initial symmetry breaking process (Wedlich-Soldner and Li, 2004).

After symmetry breaking at the initiation of budding, a polarized distribution of Cdc42 is stably maintained to ensure rapid growth of a unique bud for cell division. Although the Cdc42 polar cap appears stable, individual molecules of Cdc42, as well as the GEF Cdc24 and the adaptor protein Bem1, are highly dynamic, as shown by fluorescence recovery after photobleaching (FRAP) experiments (Wedlich-Soldner et al., 2004). Cdc42 exhibits a considerable membrane diffusion rate of 0.036 μ^2/s, measured using a mutant, $Cdc42^{Q61L}$, which is stably associated with the membrane and unable to enter the cytosol (Marco et al., 2007). To explore how a stable cap of $Cdc42^{Q61L}$ can be dynamically maintained, a mathematical model was built to describe balance of flux due to $Cdc42^{Q61L}$ membrane diffusion, internalization and polarized delivery (Marco et al., 2007). This analysis concluded that the rate of internalization of $Cdc42^{Q61L}$ was optimized to achieve maximum polarity.

While the above work provides a useful framework for understanding how the polarized distribution of a membrane protein can be maintained at a cortical domain in a dynamic manner, it did not explain how cells maintain the dynamic distribution of Cdc42 in its native form. The fluorescence recovery rate of wild-type (WT) Cdc42 in FRAP measurements is an order of magnitude higher than that of $Cdc42^{Q61L}$, due in part to the rapid exchange of Cdc42, but not $Cdc42^{Q61L}$, molecules between the membrane and cytosolic pools (Wedlich-Soldner et al., 2004). This result implicates a possible role for Rdi1, the lone guanine-nucleotide dissociation inhibitor (GDI) for Rho family GTPases in yeast, in rapid Cdc42 recycling. GDI proteins are known to play a role in maintaining soluble GTPases in the cytosol through their ability to bind the GTPase's COOH terminal prenyl group (Bustelo et al., 2007; DerMardirossian and Bokoch, 2005; Johnson et al., 2009). In yeast, Rdi1 has been shown to interact with Cdc42 at the membrane, extract Cdc42 and lead to an increase in its abundance in cytosolic fractions (Cole et al., 2007; Koch et al., 1997; Masuda et al., 1994; Richman et al., 2004; Tiedje et al., 2008).

In this study, through both experimental exploration and mathematical modeling, we show that Rdi1 indeed plays an active role in fast Cdc42 recycling. A combination of the Rdi1-mediated recycling pathway with the actin-mediated endocytic recycling, which exhibit very different dynamic constants, determines the steady-state Cdc42 distribution. The dual pathway model predicts that windows of the two recycling pathways must overlap spatially and be of similar sizes. The internalization rates for WT Cdc42 are not necessarily optimized for polarity but are instead tuned to give rise to different Cdc42 distributions that correlate with distinct morphogenetic fates.

Results

Cdc42 in budding cells is recycled at the polarized site via two mechanisms

We began the study by testing the possibility that the yeast GDI, Rdi1, known to play a role in maintaining cytosolic Cdc42, is involved in fast Cdc42 recycling. GFP-Cdc42 was introduced under its native promoter into *Δrdi1* mutant yeast cells, and FRAP data was obtained. For simplicity, "GFP" is omitted hereafter when referring to fluorescently tagged Cdc42 or Cdc42 mutant proteins, as GFP was the only fluorescent tag for Cdc42 used in this study. GFP-Cdc42 is functional as it can fully rescue growth in *Δcdc42* background (Roland Wedlich-Soldner, unpublished observation).

As in the previous work (Wedlich-Soldner et al., 2004), we focused on the polar cap of Cdc42 prior to bud emergence in a dividing cell population (Fig. 1A) to avoid data heterogeneity due to different cell-cycle stages. To determine the quantitative relationship between recycling parameters and the shape of Cdc42 steady-state distribution, we focused on cells that had already formed a stable Cdc42 polar cap. Cdc42 in *Δrdi1* cells exhibited a drastically reduced FRAP rate ($\tau = 1 / t_{1/2}$) compared to Cdc42 in WT cells (Fig. 1B,C) ($p < 10^{-10}$). The recycling defect of Cdc42 in *Δrdi1* can be mimicked by the $Cdc42^{R66E}$ mutant, which does not bind GDI (Gibson and Wilson-Delfosse, 2001) ($p = 0.3$) (Fig.1D). Treatment of WT cells with Latrunculin A (LatA) to remove the actin-dependent recycling pathway slowed recovery rate, as previously described (Wedlich-Soldner et al., 2004), while treatment of *Δrdi1* cells with LatA to depolymerize actin further reduced τ. Membrane fluorescence did eventually recover under these conditions (see below); however, these measurements are not easily comparable to WT or *Δrdi1* cells as the Cdc42 polar cap rapidly dissipated in *Δrdi1* cells treated with LatA, yielding non-polarized cells (Fig. 1E). This residual recovery persisted in the presence of cyclohexamide and thus is not a result of new protein synthesis (data not shown). The finding that Cdc42 remained polarized in either *Δrdi1* cells, or WT cells treated with LatA, but not in *Δrdi1* cells treated with LatA (1E and 1F, and Supplemental Fig. 1A), suggests that Rdi1 and actin play redundant but essential roles in maintaining Cdc42 polarization.

As LatA disrupts both actin cables and actin patches, the latter being endocytic structures, we asked if endocytosis is important for Cdc42 recycling by using the temperature sensitive *arp3-2* mutant (Winter et al., 1997). This mutant disrupts the Arp2/3 complex, the actin nucleation factor required for assembly of actin patches, at the non-permissive temperature 35° C. Similar to the effect of LatA alone, Cdc42 recycling was slowed in *arp3-2* at 35°C. Recycling of $Cdc42^{R66E}$ in arp3-2 was also impaired at 35°C, but not at the permissive temperature (Fig. 1D). The recycling rate of Cdc42 in WT cells was roughly the sum of the rate in LatA-treated or *arp3-2* cells with that of Cdc42 in *Δrdi1* or $Cdc42^{R66E}$ (Supplemental Fig. 1B). These data suggest that endocytosis and the GDI work in parallel to control Cdc42 recycling at the polar cap in WT cells. The GDI-based mechanism accounts for fast recycling of Cdc42, while endocytosis represents a slow recycling pathway.

Overview of the steady-state model of Cdc42 polar cap

In order to understand at a quantitative level how each and both recycling pathways contribute to the dynamic maintenance of a Cdc42 polar cap, we used an approach that combined quantitative imaging with mathematical modeling. The model shares the same framework as the previous one (Marco et al., 2007) but has several differences. As in the previous model, the flux of Cdc42 is governed by membrane diffusion (D_f), a window in the plasma membrane where Cdc42 is delivered to the cortex from the internal pool with rate (h), and the rate of internalization of Cdc42 from the cortex inside (m) and outside (n) this window (Fig. 2A, equation 1, and Supplemental Information). The assumption of a discrete window for polarized delivery is a simplification of the reality but is justified based on the sharp polarized distribution

of structures involved in Cdc42 recycling (Supplemental Fig. 2A) and excellent fit between model output and experimental measurements (see below).

We used a combination of (FRAP) and imaging experiments to extract model parameters (Supplemental Information and Supplemental Fig. 2B). We then applied these model parameters to a steady-state version of equation 1 to examine the effect of the parameters on the steady-state distribution of Cdc42, after the initial establishment of polarity. In the case of WT Cdc42, the model had to be expanded from the previous version (Marco et al., 2007) to describe two recycling pathways (Fig. 2B,C). Each of above parameters, with the exception of D_f, has in theory two values, each corresponding to one of the pathways (Fig. 2B,C). D_f was held constant between the two pathways, as previous analysis suggested that this was largely governed by the prenyl group that anchors Cdc42 into the membrane (Marco et al., 2007). As opposed to the previous model, *m* and *n* were assessed separately in this study. *m* was also independently validated by inverse FRAP (iFRAP) (see below). Before considering the model of dual pathways, we first assessed each pathway individually: *Δrdi1* cells enabled isolated analysis of Cdc42 polar cap maintained by actin-based recycling, while LatA treatment to remove actin allowed specific assessment of the Rdi-dependent mechanism.

Modeling the steady-state Cdc42 cap through actin or Rdi1-mediated recycling

To assess the situation where there is only actin-based recycling (Cdc42 in *Δrdi1*), the delivery window was determined by measuring the distribution of the formin protein Bni1 on the plasma membrane (Fig. 3a). Bni1 nucleates the formation of actin cables and stays at actin barbed ends as the filaments elongate (Evangelista et al., 2003). Therefore, the Bni1 distribution on the cortex is likely to correlate with the ends of actin cables and thus the window of cable-based delivery. The average full width half-max (FWHM) of a Gaussian fit of the perimeter line-scan of cells expressing Bni1-GFP was 13% of the cell perimeter in WT cells, thus the total width of the actin-based delivery window was roughly 26% of the perimeter (Fig. 3A). The Bni1 distribution was not dramatically changed in *Δrdi1* cells or upon expression of $Cdc42^{Q61L}$ (Fig. 3A). The Bni1 distribution was slightly narrower than polarized Cdc42 (Fig. 3A, Supplemental Fig. 3), consistent with spreading due to membrane diffusion of Cdc42 once delivered to the cortex.

Using this delivery window size, we applied the partial differential equation-based model to our time-dependent FRAP data and the relative integrated membrane-bound Cdc42 intensity inside and outside this window to arrive at a unique solution of *m*, *n*, and *h* for each cell (Fig. 3D) (see Supplemental Information). An output of the model is the amount of internal Cdc42 relative to the total Cdc42 (G_c), (see Supplemental Information). Comparison of the computed G_c to the experimentally measured value provides an independent validation of the model and was remarkably accurate on a cell to cell basis (Fig. 3B).

As a second validation, values of internalization rate inside the delivery window (*m)* obtained from the modeled FRAP data were compared to fluorescence loss rates in independent iFRAP experiments. In iFRAP, the internal (cytosolic + internal membrane-bound) Cdc42 was photobleached, and the rate of fluorescence decrease at the polar cap was monitored as molecules left this region (example – Fig. 3C). As opposed to FRAP, which is defined by a combination of events described by equation 1, we expect that the rate of fluorescence loss in iFRAP is an approximation for *m*, because only 10 to 20% of Cdc42 molecules are present in the polar cap while a vast abundance of Cdc42 molecules take part in the equilibrium between cytosol and the cap. Indeed, the rate of Cdc42 fluorescence loss measured by iFRAP matched well with *m* values obtained by modeling FRAP data (Fig. 3D).

The model predicted the ratio of Cdc42 internalization rates by the actin-based pathway inside and outside the delivery window (*m*/*n*) to be 2.8 ± 0.3. Due to a low amount of Cdc42 outside

the delivery window and thus a reduced signal to noise in fluorescence measurements, it was not possible to validate internalization rate outside the window (*n)* by iFRAP. To assess the ratio *m*/*n* experimentally, we measured the density of actin patches inside and outside the delivery window with two-color confocal imaging of cells expressing Bni1-GFP and mCherry-tagged Arc40, a subunit of the Arp2/3 complex concentrated in actin patches. The ratio of actin patches inside to outside the Bni1-defined window was 3.1 ± 0.2 (n=18) (Fig. 3E), in close agreement with the ratio of *m/n* calculated by the model (p = 0.35). Along with the FRAP data in the *arp3-2* strain, this supports the idea that Cdc42 is internalized by endocytosis through actin patches at rates proportional to the local density of actin patches. The strong polarization of Bni1 (Fig. 3A) and actin patches (Supplemental Fig. 2) justifies the use of a discrete, window–based model for describing steady-state polarity.

As opposed to the actin-dependent recycling system, where the window of delivery is marked by the formin Bni1, the basis of the delivery window size for the Rdi1 pathway was unknown. To explore the simplest possibility, we analyzed Cdc42 FRAP data in cells treated with LatA with the model using the same window size as the actin-based pathway. Recycling parameters were calculated by applying the model to the FRAP data and are shown in Fig. 3D. *h* for the Rdi1 pathway was higher than that for the actin-based pathway, as was *m*, while *n* was similar between the two pathways. Values of G_c as an output of the model matched the experimentally measured values well (Fig. 3B). The model-calculated values of *m* were slightly higher than, though in a same range with, rates from iFRAP in cells treated with LatA (Fig. 3D). We also examined the possibility that the Rdi1-recycling window was larger or smaller in the dual recycling model (see below).

A model of the steady-state Cdc42 polar cap maintained by dual recycling

To explore how the two recycling mechanisms work together to dynamically regulate Cdc42 distribution in the polar cap of WT cells, we again first applied the simplest possible scenario: that the two recycling mechanisms are spatially overlapping and employ concentric delivery windows of the same size (depicted in Fig. 2B). When two overlapping windows of the same size are considered mathematically, their rates become additive (see Supplemental Information), i.e., the overall recycling parameters of *m*, *n*, and *h* for WT Cdc42 are expected to be the sum of parameters from the two individual pathways (Fig. 2B).

With the above consideration, we applied the single pathway model to FRAP data of Cdc42 in WT yeast cells, using a window size of 26% of the perimeter. Values of G_c predicted from the model agreed well with experimental G_c measurements (Fig. 3B). The average value of G_c for Cdc42 in WT cells (61%) was qualitatively consistent with the high percentage of cytosolic Cdc42 found in a fractionation experiment (Wedlich-Soldner et al., 2004). Interestingly, we indeed observed that the values of *n*, *h*, and *m* calculated from Cdc42 FRAP and imaging data in WT yeast cells using a single pathway model were statistically equivalent to the distributions obtained by simply adding all possible combination of parameters measured for *Δrdi1* cells and cells treated with LatA (Fig. 3D). In addition, the values of *m* predicted from the model for treatment of WT Cdc42 with a single pathway or *m* resulting from the sum of m_1 and m_2 from the two individual pathways both closely matched internalization rate of Cdc42 in WT cells measured independently by iFRAP (Fig. 3D). This analysis suggests that dynamics of Cdc42 in WT cells can be adequately described experimentally and mathematically as a sum of the Rdi1-dependent and actin-dependent pathways.

While the choice of identical windows for the two pathways has so far enabled excellent agreement between model predictions and experimental measurements, we explored the possibility that the Rdi1-based exchange window may be smaller or larger than the actin-based delivery window (Fig. 2C). We reworked the model to allow for combination of two pathways of different sizes (Fig. 2C), with the window size of the actin-dependent delivery held constant

(see eqs. S18-S22, Supplemental Information). Because the rate of internalization measured for Cdc42 in WT cells by iFRAP and the overall recycling rate as measured by FRAP were roughly the sum of the rates for the individual pathways (Fig. 1, Fig. 3D, and Supplemental Fig. 1), and the Cdc42 polar caps are generally symmetric, we know to good approximation that the actin-dependent and Rdi1-dependent recycling windows are concentric. Furthermore, if the individual recycling pathways are described correctly, their combination should effectively recapitulate the observed Cdc42 distribution in WT cells.

FRAP data of LatA treated cells were modeled with the use of a smaller or larger window than previously employed. We then combined the new parameters of the Rdi1-recycling pathway with the actin-pathway parameters in a dual recycling pathway scenario, and calculated steady-state distributions (Fig. 4). Combination of parameters from the two pathways with a smaller Rdi1 pathway window than that of the actin pathway resulted in a predicted Cdc42 cortical distribution with a valley in Cdc42 intensity at the center of the cap (Fig. 4D,E). This pattern of Cdc42 distribution was not observed in WT cells. If the Rdi1-based delivery window was assumed to be larger than that of the actin-based recycling, the resultant WT Cdc42 distribution upon combination of the pathways was very wide, covering nearly half of the membrane (Fig. 4D,E). This wide distribution also was not observed experimentally (Supplemental Fig. 3). In addition, the average G_c values calculated from the resultant steady-state distribution after combination of the smaller or larger Rdi1-mediated recycling window with the actin-recycling window were 0.34 and 0.42, respectively, both far outside the range of experimentally measured G_c for Cdc42 in WT cells (average 61%) (Fig. 3B). In contrast, direct combination of recycling parameters from individual actin and Rdi1-dependent processes using identical window sizes (26% of perimeter) produced a distribution identical to that obtained by modeling FRAP data of WT Cdc42 with a single window model (as depicted in Fig. 2A), (Fig. 4E). We note the steady-state distributions calculated from the model parameters fit the experimental distributions well, despite the noise in the experimental distributions (Fig. 4F). Based on these analyses, the only way to accurately represent Cdc42 distributions in WT cells through two independent recycling pathways is to assume concentric windows of similar sizes.

One point of interest is the observed fluorescence recovery, albeit slow, even in the absence of both Rdi1 and actin (Fig. 1C,D). To assess the potential impact of a third recycling pathway on our system, the model was revised to include a large window encompassing the entire cell surface, as recovery by this pathway was uniform and did not maintain polarity (see Supplemental Information section 2.5). We applied the revised model to *Δrdi1* cells treated with LatA, and the resultant value of h was very small: 0.00023 ± 0.00005 [$1/(\mu^2 * s)$] (Supplemental Fig. 4). The order of magnitude lower value of the delivery rate observed here compared to those for the actin or Rdi1-based pathway allowed us to neglect this mechanism in the model.

The Cdc42 GTPase cycle regulates the two recycling pathways

The result that two windows of Cdc42 recycling must colocalize on the cortex and be of similar size is a useful and unexpected finding of the model. A potential mechanism underlying their colocalization may be that both pathways rely upon the Cdc42 GTPase cycle, since Cdc42 mutants locked in either nucleotide bound state ($Cdc42^{Q61L}$ or $Cdc42^{D57Y}$) exhibited much reduced FRAP rates compare to WT Cdc42 (Wedlich-Soldner et al., 2003; Wedlich-Soldner et al., 2004). The mutant FRAP rates were not further reduced in the *Δrdi1* mutant (Fig. 5A), suggesting Rdi1 no longer participates in the slow recycling of these mutants.

We tested if $Cdc42^{Q61L}$ and $Cdc42^{D57Y}$ mutant proteins might be deficient in GDI-complex formation in the cytosol using live-cell fluorescence cross correlation spectroscopy (FCCS) (Bacia et al., 2006) (for methods, see Supplemental information). FCCS assesses protein complex formation by measuring co-diffusion, or cross-correlation, of red- and green-labeled

species. We showed previously that cross-correlation between mCherry and GFP-tagged proteins expressed at their endogenous levels in live yeast cells is an effective method to quantitatively examine cytosolic interactions (Slaughter et al., 2008; Slaughter et al., 2007). Strong cross-correlation (20%) was indeed observed between GFP-Cdc42 and Rdi1-mCherry in the cytosol of polarized yeast cells, compared to that of the negative control of unlinked GFP and mCherry (~4%). The positive control of linked GFP-mCherry (~ 45%) was less than 100% due likely to incomplete folding or dark states of auto-fluorescent proteins; also see (Slaughter et al., 2007) (Fig. 5B,C). We note that Rdi1-mCherry is an active protein, at least in its ability to rescue rapid recycling of Cdc42 in the *Δrdi1* background (data not shown). The observed cross-correlation of Rdi1-mCherry with GFP-Cdc42 was abolished by the R66E or C188S mutation of Cdc42, both expected to disrupt the interaction of Cdc42 with GDI (Gibson and Wilson-Delfosse, 2001; Koch et al., 1997; Masuda et al., 1994). Surprisingly, both GFP-Cdc42^{Q61L} and GFP-Cdc42^{D57Y} exhibited drastically reduced levels of cross-correlation with Rdi1-mCherry, suggesting that formation of the cytosolic Cdc42-Rdi1 complex *in vivo* is dependent on an active GTPase cycle.

To determine if defects in the GTPase cycle also affect the actin-based recycling of Cdc42, we used the model to analyze FRAP results of Cdc42^{Q61L} in the *Δrdi1* background. Values of G_c predicted with the model for Cdc42^{Q61L} agreed well with experimentally measured values and were lower than G_c values for WT Cdc42 (Fig. 3B). The internalization rates inside the window (*m)* predicted for Cdc42^{Q61L} in *Δrdi1* were much lower than those for WT Cdc42 in *Δrdi1* cells and agreed well with experimentally measured internalization rates from iFRAP, while the rate of delivery (*h)* for Cdc42^{Q61L} was only slightly lower compared to that of WT Cdc42 in *Δrdi1* (Fig. 3D). Interestingly, while *m* was reduced for Cdc42^{Q61L}, the rate of internalization outside the window (*n*)predicted for Cdc42^{Q61L} in *Δrdi1* was statistically indistinguishable from the *n* value for WT Cdc42 in *Δrdi1* ($p = 0.61$) (Fig. 3D). These results suggest that the defect in Cdc42 GTPase activity impaired Cdc42^{Q61L} recycling via endocytosis within the delivery window, but had little effect outside the delivery window.

One potential mechanism by which the Q61L mutation could reduce the Cdc42 recycling rate is stabilization of the interaction of Cdc42-GTP with its effectors, should the effector-bound Cdc42 molecules be protected from endocytosis. To test this hypothesis, we introduced the mutation T35A to Cdc42^{Q61L}, which was shown to disrupt binding of CRIB-domain-containing effectors (Gladfelter et al., 2001), though T35 may also cause a structural change of the entire effector loop in the GTP-bound state of Cdc42 or Ras (Adams and Oswald, 2007; Spoerner et al., 2001). Supporting our hypothesis, Cdcc42^{Q61L,T35A} was recycled at a much more rapid rate than Cdc42^{Q61L}, whereas the T35A mutant did not improve the recycling of the GDP-bound Cdc42^{D57Y}, which does not bind effectors (Fig. 5A). Moreover, recycling of Cdc42^{Q61L,T35A} was not changed further in the *Δrdi1* mutant cells, suggesting that recycling of this mutant was through endocytosis in an Rdi1-independent manner (Fig. 5A). Taken together, the results described above suggest that the GTPase cycle of Cdc42 controls both pathways of recycling, by allowing the formation of the complex with Rdi1 and by triggering the release of effectors to allow internalization through the endocytosis. The latter mechanism was further supported by the effect of overexpression of the effector Gic2 on recycling (see below).

If the Cdc42 GTPase cycle is required for both recycling pathways, the recycling windows may co-localize with regulators of the Cdc42 GTPase cycle. While the GEF Cdc24 promotes the exchange of GDP for GTP on Cdc42, the GTPase activity of Cdc42 is controlled by several partially redundant GAP proteins (Knaus et al., 2007; Sopko et al., 2007; Zheng et al., 2007). We examined two of these GAPs, Bem2 and Bem3, because they localize to the bud tip and have been shown to regulate Cdc42 during bud formation (Knaus et al., 2007). Indeed, in the *Δbem2Δbem3* double mutant, Cdc42 recycling rate was significantly reduced (Fig. 5A).

Furthermore, measurement of GFP-tagged GAP or GEF proteins showed that these proteins were concentrated as polar caps in polarized G1 cells that displayed similar widths as that of Bni1 (Fig. 5D). Strains expressing both Bni1-GFP and Bem2-mCherry or GFP-Cdc42 and Bem2-mCherry further demonstrated nearly perfect colocalization (Fig. 5E). This colocalization was unaffected in *Δrdi1* cells (data not shown). In addition, Bem2 and Rga1 (but not Bem3 (Knaus et al., 2007)) remained strongly polarized at the polar cap upon LatA treatment (data not shown), consistent with the idea of the Rdi1 window remaining in place independently of actin. The above data support the idea that the Cdc42 GTPase cycle is required for both recycling pathways and therefore may underlie the co-localization of the two recycling pathways.

Relationship between the rate of internalization and strength of polarity

The earlier model of $Cdc42^{Q61L}$ maintenance in G1 arrested cells predicted a non-monotonic relationship between the rate of internalization and polarity, measured as the ratio of the Cdc42 distribution peak height over peak width (Marco et al., 2007). It was found that the observed rate of internalization inside the window (*m*) falls on the value that correlated with maximal polarity. To investigate if polarity is also optimized by the rate of internalization of WT Cdc42 during the physiological process of budding, we calculated a steady-state distribution (equation S5, in non-dimensional units) from average parameters of *m*, *n*, and *h* for each condition, from which polarity was calculated as previously defined (peak height divided by window width). To compare our results directly to the previous model, *m/n* ratios were fixed to the average of the data obtained for each specific condition and the calculated theoretical polarity was plotted as a function of *m*. This analysis showed that for $Cdc42^{Q61L}$ in *rdi1*, the observed internalization rate inside the window (*m)* was indeed found to be optimized for maximum polarity, consistent with the previous finding (Marco et al., 2007). However, this optimization was not found for WT Cdc42 recycled by either individual pathway or by dual pathways. In each of these cases, polarity maximum fell to the left of the measured values of *m*. In other words, internalization rates were faster than those that would result in polarity maximum.

Since similar values of internalization rate outside the window (*n)* for the actin-dependent recycling pathway (in *Δrdi1*) were obtained for Cdc42 and $Cdc42^{Q61L}$, it was more reasonable to compare the two forms of Cdc42 with *n* held constant as opposed to a constant *m*/*n* ratio as previously assumed. Fig. 6E plots polarity as a function of *m* for fixed *n* and *h* (note the measured values of *h* were similar but not identical for the two conditions shown here and this plot used their average). The resulting plot demonstrates that for these values of *n* and *h*, polarity will increase monotonically with reduced *m*. This comparison can be extended to include also the recycling of Cdc42 by the Rdi1 pathway (i.e. in the presence of LatA). In this case, the internalization rate outside the window (*n)* was similar between all three conditions, but the rate of delivery (*h)* was different, making possible a three dimensional plot examining polarity as a function of *m* and *h* for fixed *n* (Supplemental Fig. 5A). The 3D plot confirms the generality that a reduced rate of internalization inside the window relative to other parameters increases polarity. To explore the relationship of all model parameters to polarity in general, we searched parameter space for combinations of *m*, *n*, and *h* that would satisfy specified requirements for a polarized system at three values of D_f: 0.36, 0.036, and 0.0036 μ^2/sec. The three-dimensional parameter-space plot and its projections are shown in Supplemental Fig. 5B,C, and the result is discussed in detail in Supplemental text.

Recycling parameters affect the shape of the Cdc42 polar cap distribution and subsequent morphogenesis

As the observed rates of internalization of WT Cdc42 do not result in maximal polarity, we tested whether these rates might instead be related to adaptation to specific morphogenetic functions. We first compared the steady-state distribution of Cdc42 or $Cdc42^{Q61L}$ on the cortex,

modeled using average values of *m*, *n*, and *h* obtained for each of the conditions indicated (equation S5) (Fig. 7A). The height of the distribution was increased for $Cdc42^{Q61L}$ relative to other conditions examined. This is observed as an increase in the amount of Cdc42 inside the window relative to the total Cdc42. At the opposite end, Cdc42 in WT cells treated with LatA (thus recycled by the Rdi1 pathway) had a reduction in the amount of Cdc42 within the window. The qualitative trend of the above comparison of the modeled Cdc42 distributions was also confirmed with imaging of Cdc42 intensity within the window relative to total Cdc42 (Fig. 7B).

Interestingly, the predicted WT Cdc42 distribution had a distinct shape from that of $Cdc42^{Q61L}$: the WT Cdc42 membrane distribution was broader inside the window than the distribution of $Cdc42^{Q61L}$, giving the former a more box-like shape. To quantify this difference through a single parameter, we chose the slope value at half the distance from the cap center to the window edge in the average WT Cdc42 distribution and termed this the critical slope. We then calculated the distance from the center of the polar cap to where this slope was achieved for each modeled cell. The farther from the center of the cap that the membrane distribution reaches this critical slope, the more 'box-like' the distribution is inside the cap. This method of quantification allows for examination of curves without the need to force their fit to a function. The pointed nature of the distribution for $Cdc42^{Q61L}$ is revealed in this analysis compared to other conditions examined (Fig. 7C).

As Cdc42 establishes the site of polarized secretion in yeast through multiple downstream mechanisms (see Introduction), the shape and strength of its distribution is likely to be the main determinant of the shape of polarized growth. The more box-like polar cap observed with wild-type Cdc42 compared to that of $Cdc42^{Q61L}$ may ensure that growth is better spread out within the polar cap to form a round rather than pointed bud. To examine this possibility, we labeled live cell surfaces with fluorescent manno-protein marker concanavalin-A (Tkacz et al., 1971; Tkacz and Lampen, 1972). Using confocal imaging, we indeed observed more pointed buds for cells expressing $Cdc42^{Q61L}$ compared to cells expressing WT Cdc42 (Fig. 7D). This effect was not due to a difference in the expression levels of Cdc42 and $Cdc42^{Q61L}$ (Supplemental Fig. 6A). The difference in bud shape was quantified by examining the relationship between the length and width of buds. Larger length relative to width was observed for cells expressing $Cdc42^{Q61L}$ than those expressing WT Cdc42 in buds of all sizes (Fig. 7D-F). While in large buds this could be explained by a lack of depolarization in cells expressing $Cdc42^{Q61L}$ at a later cell cycle stage, the difference was statistically significant in small buds with widths less than 3 microns (Fig. 7F). This result suggests that a higher internalization rate for WT Cdc42 within the delivery window is important for achieving a round bud morphology.

To test further if tuning *m* can modulate bud morphology, we took FRAP data and modeled Cdc42 recycling in the presence of an increased level of the CRIB domain-containing effector Gic2 (Brown et al., 1997; Chen et al., 1997) expressed under the *GAL1* promoter, since effector binding may negatively regulate Cdc42 internalization (Fig. 5). Gic2 overexpression indeed slowed recycling of Cdc42 (Supplemental Fig. 6B). Moreover, the internalization rate *m* was reduced while the internalization rate outside the window *n* was unchanged (Supplemental Fig. 6B). Again, we find that reduction in *m* relative to *n* resulted in a pointed steady-state Cdc42 distribution, and subsequent pointed morphology (Supplemental Fig. 6C,D). The value of *h* was also reduced, though reduction in *h* serves only to reduce the overall amplitude of the steady-state distribution but does not affect distribution shape (for given *m*, *n*, and cell size) (Supplemental Fig. 6E).

The pointed cell morphology due to experimentally reducing the internalization rate *m* by either expressing $Cdc42^{Q61L}$ or overexpressing the effector Gic2 led us to ask if tuning of the internalization rate occurs naturally as a means to achieve a pointed morphology in yeast. For

example, in mating, a sharp shmoo tip is desired for efficient cell fusion (Madden and Snyder, 1998). We applied the model to FRAP data of cells arrested with the mating pheromone α-factor (Fig. 7G). A slightly smaller window size was used (17%), as measured from the Bni1-GFP distribution in these cells (Supplemental Fig. 6F). The delivery rate (*h)* and internalization rate outside the window (*n)* for Cdc42 were found to be similar between pheromone-arrested cells and cycling cells, whereas the internalization rate inside the window (*m*) was significantly reduced (Fig. 7H). This reduction in *m* was verified by independent iFRAP measurements of Cdc42 (red points in Fig. 7H).

We next determined if the reduction in internalization rate, *m*, observed for WT Cdc42 in pheromone-arrested cells compared to that in cycling cells was due to a change in actin or Rdi1-based recycling. Interestingly, the iFRAP rate in *Δrdi1* cells showed no difference between cycling cells and shmooing cells (Fig. 7I), while a reduced rate of internalization was observed in shmooing versus cycling cells upon treatment with LatA (Fig. 7I), recapitulating the difference in Cdc42 internalization rates between WT shmooing and cycling cells. This data suggests that in the case of pointed shmoos, it is the Rdi1 pathway that is modulated to achieve a slower Cdc42 internalization rate, leading to a pointed Cdc42 distribution relative to cycling cells (Fig. 7C,J, Supplemental Fig. 6H) and subsequent characteristic shmoo morphology.

Discussion

The results presented above demonstrate that Cdc42 is recycled through two mechanistically distinct pathways, one involving membrane trafficking, and the other requiring the conserved Cdc42 regulator, GDI. While GDI is well known to bind and extract Cdc42 from the membrane into the cytosol (Cole et al., 2007; Hoffman et al., 2000; Koch et al., 1997; Masuda et al., 1994; Richman et al., 2004; Tiedje et al., 2008), our finding that Rdi1 mediates a fast pathway of Cdc42 recycling that contributes to the dynamic maintenance of Cdc42 polarized localization suggests that Rdi1 plays a positive, as opposed to inhibitory, role in Cdc42-based functions. The lack of obvious growth phenotype of the Rdi1 deletion mutant strain in cycling cells may be explained by the presence of a redundant pathway for Cdc42 recycling (endocytosis). However, inhibition of both pathways led to rapid loss of Cdc42 polarity.

Our data suggest that the mechanisms by which the GTPase cycle of Cdc42 facilitates internalization of Cdc42 through the dual pathways are complex. Using FCCS analysis, a strong interaction of Rdi1 with Cdc42 was observed in the cytosol of live yeast cells, consistent with its proposed mechanism of action. However, formation of the Rdi1-Cdc42 complex was drastically reduced by mutations that lock Cdc42 in the GTP or GDP bound forms. This result suggests that *in vivo* the GTPase cycle of Cdc42, but not a particular nucleotide-bound form, is important for the formation of Rdi1-Cdc42 complex, and that not all Cdc42 molecules in the mobile pool are free to bind Rdi1. Recent *in vitro* experiments in lipid bi-layers found that the rate of dissociation the Cdc42-GDI complex from the membrane is unaffected by the nucleotide-bound state of Cdc42, even though the affinity of GDI for Cdc42 is nearly 10 fold higher for GDP bound Cdc42 than GTP bound (Johnson et al., 2009). Our results suggest that GTPase hydrolysis presents another layer of regulation *in vivo* where bound regulators or effectors may prevent the formation of the Cdc42-GDI complex and corresponding Cdc42 dissociation from the membrane.

The GTPase cycle also regulates Cdc42 recycling via endocytosis. The observation that the effector-binding mutation T35A increased the recycling rate of $Cdc42^{Q61L}$ to near that of WT Cdc42 in *Δrdi1* cells suggests that simply abrogating effector binding, without restoring GTPase activity, was sufficient to enable Cdc42 to be recycled more efficiently through endocytosis. Although T35A might also lead to a gross structural change in Cdc42 that can

affect its interaction with other regulatory proteins, the effect of overexpression of Gic2 supports the possibility that binding to specific or a wide range of effectors could protect Cdc42 from endocytic internalization. However, this mechanism does not explain the slow recycling of $Cdc42^{D57Y}$, which is not expected to bind effectors and consequently did not exhibit enhanced recycling in the presence of the T35A mutation. Slow recycling of $Cdc42^{D57Y}$ relative to $Cdc42^{Q61L,T35A}$ suggests that Cdc42 must be in the GTP-bound active form in order to efficiently enter or stimulate the formation of endocytic structures, consistent with the known role of active Cdc42 in stimulating the formation of cortical actin patches (Lechler et al., 2001; Li et al., 1995).

The presence of two parallel pathways for Cdc42 recycling underscores the importance of this process and provides robustness for dynamically maintained cell polarity. In addition, the parameters of these recycling pathways can be tuned to control the shape of the Cdc42 distribution. Only wild-type Cdc42 recycled through dual pathways was able to maintain relatively high polarity as well as a 'box-like' shape that ensures growth of a round bud that is characteristic of the organism and may be optimized for receiving segregating organelles and nuclear materials during mitosis. In contrast, the reduced internalization rate inside the delivery window in $Cdc42^{Q61L}$ – expressing cells results in a sharper Cdc42 peak that leads to a pointed bud shape. More interestingly, a reduction in the internalization rate inside the delivery window (*m*) was observed in cells undergoing pheromone response and predicts a sharper Cdc42 distribution than that in cycling cells. While other factors could also be involved, it is likely that the sharper Cdc42 distribution contributes to the pointed shmoo shape, which is required for efficient mating.

Taken together, our results suggest that parameters of Cdc42 recycling in yeast, especially the internalization rate within the polarized region, are adapted not to achieve maximum polarity, but to fulfill specific morphogenetic outcomes that may be advantageous to either vegetative growth or mating (Fig. 7K). The observed difference between $Cdc42^{Q61L}$ and wild-type Cdc42 may help explain why Rho GTPases are not simply membrane proteins but instead are evolutionary conserved, nimble regulators of cell polarity. By involving the GTPase cycle in their rapid recycling, the dynamic parameters of Cdc42 recycling can potentially be tuned through GAPs, GEFs and effectors. These in turn are targets of further upstream signals, thus allowing the GTPase protein distribution to adapt to different downstream morphogenetic requirements. As Cdc42 and regulators of its recycling are all highly conserved, the principles observed in this study may be extended to other systems of polarized morphogenesis.

Experimental Procedures

Yeast culture

Yeast strains used in this study are listed in Supplemental Table 1. Yeast cells were grown in synthetic complete media to mid-log phase prior to analysis. For experiments with Latrunculin-A (BioMol), 100 μM LatA was added for 10 to 15 minutes prior to data acquisition. Yeast cells were immobilized on glass for analysis. For experiments using the *GAL1* promoter for Cdc42, cells were grown to mid-log phase in synthetic media with raffinose, and then induced with 2% galactose for 1.5 to 2 hours. For overexpression of Gic2 with p*GAL1*, 2.5 hours of induction were used. For studies in pheromone-arrested cells, 75 μM α-factor (Pi Proteomics) was added for 1.5 hours. For examination of bud shape, 200 μL cells were treated with 15 μL of 1 mg/mL FITC-Concanavalin-A for 30 minutes. The cells were washed twice with PBS, and then imaged.

In most experiments, GFP-Cdc42 was controlled under the *CDC42* promoter; however, because $Cdc42^{Q61L}$ is dominant lethal, the inducible *GAL1* promoter was used in experiments involving comparisons with this mutant. Induction of Cdc42 expression with the *GAL1*

promoter for 90 to 120 minutes led to expression of Cdc42 proteins at a level similar to the expression level using the *CDC42* promoter (Supplemental Fig. 8).

Imaging experiments and data analysis

Confocal images were acquired with an inverted Zeiss 200m outfitted with a spinning disc confocal system (Yokagawa) and a EM-CCD (Hamamatsu C9100). FRAP and iFRAP data were acquired with this system using an attached Micro-point Mosaic bleaching system (Photonic Instruments) integrated with Metamorph acquisition software (Molecular Devices). Extraction of data from the images was performed using ImageJ software, and least-squares fitting was performed with OriginLab Pro. For determination of size of the membrane distribution to cell perimeter for Bni1, Bem2, Bem3, Rga1, and Cdc24, a linescan was drawn around the cell perimeter of a confocal slice (Fig. 3C) and fit to a Gaussian distribution. Total distribution width was approximated as two times the full width half max (FWHM) of the Gaussian distribution.

FCCS

Fluorescence cross-correlation spectroscopy (Bacia et al., 2006) data was obtained in live yeast as previously described (Slaughter et al., 2008; Slaughter et al., 2007). Briefly, GFP-Cdc42 and Rdi1-mCherry was excited using the 488 nm and 561 nm laser lines, respectively, of a Zeiss Confocor 3. Emission filters were BP 505-540 and LP580 for the red and green channels, respectively. An emission dichroic of HFT590 was used, compared to the HFT565 used previously, to minimize cross-talk from the green to red channel. Correlation curves were fit and amplitudes of the correlation curves were used to calculate a %bound fraction of the two species (Rigler et al., 1998).

General model

We consider a model of Cdc42 protein dynamics on the surface of a polarized yeast cell (Marco et al., 2007). The dynamics of the distribution of Cdc42 along the membrane can be represented by equation 1, where $f(r,\phi,t)$ denotes the surface (membrane) density of Cdc42, $D_f\Delta f$ describes the diffusion along the membrane, and m represents the internalization rate inside the delivery window. The parameter n is the internalization rate outside the window, h is the rate of delivery of molecules to the polar cap, and F_c is the amount of cytosolic (or internal) Cdc42 (see Fig. 2). χ equals 1 inside the confines of the window and equals 0 outside.

$$\frac{\partial f}{\partial t} = D_f \Delta f - m\chi f - n(1-\chi) f + h\chi F_c. \quad (1)$$

As the FRAP process is essentially non-stationary we use equation 1 as a starting point and use time dependent FRAP data along with imaging to determine model parameters (Supplemental Information). We then choose to use model parameters from FRAP data to examine a steady-state version of equation (1) for description of a polarized protein undergoing dynamic equilibrium at steady state, and not during initial stages of polarity establishment. All parameters except the diffusion coefficient are found from the combination of FRAP and steady-state imaging experiments as described in Supplemental Information.. The value of D_f of 0.036 $\mu m^2/s$ was used as published (Marco et al., 2007).

For details of imaging experiments, data analyses, and FCCS, see Supplemental information.

Supplementary Material

Refer to Web version on PubMed Central for supplementary material.

Acknowledgments

We are grateful to Giulia Rancati, Stowers Institute for Medical Research (SIMR), Sarah Smith (SIMR), Norman Pavelka (SIMR), and Roland Wedlich-Soldner (Max-Planck Institute of Biochemistry) for critical reading of the manuscript. We also thank Winfried Wiegraebe (SIMR) and Jay Unruh (SIMR) for valuable discussion. This project is supported by NIH GM057063 to RL, and NIH fellowship F32 GM077923-01A1 to BS.

References

Adams PD, Oswald RE. NMR assignment of Cdc42(T35A), an active Switch I mutant of Cdc42. Biomol NMR Assign 2007;1:225–227. [PubMed: 19636871]

Bacia K, Kim SA, Schwille P. Fluorescence cross-correlation spectroscopy in living cells. Nat Methods 2006;3:83–89. [PubMed: 16432516]

Brown JL, Jaquenoud M, Gulli MP, Chant J, Peter M. Novel Cdc42-binding proteins Gic1 and Gic2 control cell polarity in yeast. Genes Dev 1997;11:2972–2982. [PubMed: 9367980]

Bustelo XR, Sauzeau V, Berenjeno IM. GTP-binding proteins of the Rho/Rac family: regulation, effectors and functions in vivo. Bioessays 2007;29:356–370. [PubMed: 17373658]

Chen GC, Kim YJ, Chan CS. The Cdc42 GTPase-associated proteins Gic1 and Gic2 are required for polarized cell growth in Saccharomyces cerevisiae. Genes Dev 1997;11:2958–2971. [PubMed: 9367979]

Cole KC, McLaughlin HW, Johnson DI. Use of bimolecular fluorescence complementation to study in vivo interactions between Cdc42p and Rdi1p of Saccharomyces cerevisiae. Eukaryot Cell 2007;6:378–387. [PubMed: 17220465]

DerMardirossian C, Bokoch GM. GDIs: central regulatory molecules in Rho GTPase activation. Trends Cell Biol 2005;15:356–363. [PubMed: 15921909]

Etienne-Manneville S. Cdc42--the centre of polarity. J Cell Sci 2004;117:1291–1300. [PubMed: 15020669]

Evangelista M, Zigmond S, Boone C. Formins: signaling effectors for assembly and polarization of actin filaments. J Cell Sci 2003;116:2603–2611. [PubMed: 12775772]

Gibson RM, Wilson-Delfosse AL. RhoGDI-binding-defective mutant of Cdc42Hs targets to membranes and activates filopodia formation but does not cycle with the cytosol of mammalian cells. Biochem J 2001;359:285–294. [PubMed: 11583574]

Gladfelter AS, Moskow JJ, Zyla TR, Lew DJ. Isolation and characterization of effector-loop mutants of CDC42 in yeast. Mol Biol Cell 2001;12:1239–1255. [PubMed: 11359919]

Hoffman GR, Nassar N, Cerione RA. Structure of the Rho family GTP-binding protein Cdc42 in complex with the multifunctional regulator RhoGDI. Cell 2000;100:345–356. [PubMed: 10676816]

Johnson DI. Cdc42: An essential Rho-type GTPase controlling eukaryotic cell polarity. Microbiol Mol Biol Rev 1999;63:54–105. [PubMed: 10066831]

Johnson JL, Erickson JW, Cerione RA. New insights into how the Rho guanine nucleotide dissociation inhibitor regulates the interaction of Cdc42 with membranes. J Biol Chem 2009;284:23860–23871. [PubMed: 19581296]

Knaus M, Pelli-Gulli MP, van Drogen F, Springer S, Jaquenoud M, Peter M. Phosphorylation of Bem2p and Bem3p may contribute to local activation of Cdc42p at bud emergence. Embo J 2007;26:4501–4513. [PubMed: 17914457]

Koch G, Tanaka K, Masuda T, Yamochi W, Nonaka H, Takai Y. Association of the Rho family small GTP-binding proteins with Rho GDP dissociation inhibitor (Rho GDI) in Saccharomyces cerevisiae. Oncogene 1997;15:417–422. [PubMed: 9242378]

Lechler T, Jonsdottir GA, Klee SK, Pellman D, Li R. A two-tiered mechanism by which Cdc42 controls the localization and activation of an Arp2/3-activating motor complex in yeast. J Cell Biol 2001;155:261–270. [PubMed: 11604421]

Li R, Gundersen GG. Beyond polymer polarity: how the cytoskeleton builds a polarized cell. Nat Rev Mol Cell Biol 2008;9:860–873. [PubMed: 18946475]

Li R, Zheng Y, Drubin DG. Regulation of cortical actin cytoskeleton assembly during polarized cell growth in budding yeast. J Cell Biol 1995;128:599–615. [PubMed: 7860633]

Madden K, Snyder M. Cell polarity and morphogenesis in budding yeast. Annu Rev Microbiol 1998;52:687–744. [PubMed: 9891811]

Marco E, Wedlich-Soldner R, Li R, Altschuler SJ, Wu LF. Endocytosis optimizes the dynamic localization of membrane proteins that regulate cortical polarity. Cell 2007;129:411–422. [PubMed: 17448998]

Masuda T, Tanaka K, Nonaka H, Yamochi W, Maeda A, Takai Y. Molecular cloning and characterization of yeast rho GDP dissociation inhibitor. J Biol Chem 1994;269:19713–19718. [PubMed: 8051050]

Onsum MD, Rao CV. Calling heads from tails: the role of mathematical modeling in understanding cell polarization. Curr Opin Cell Biol 2009;21:74–81. [PubMed: 19167872]

Park HO, Bi E. Central roles of small GTPases in the development of cell polarity in yeast and beyond. Microbiol Mol Biol Rev 2007;71:48–96. [PubMed: 17347519]

Richman TJ, Sawyer MM, Johnson DI. Saccharomyces cerevisiae Cdc42p localizes to cellular membranes and clusters at sites of polarized growth. Eukaryot Cell 2002;1:458–468. [PubMed: 12455994]

Richman TJ, Toenjes KA, Morales SE, Cole KC, Wasserman BT, Taylor CM, Koster JA, Whelihan MF, Johnson DI. Analysis of cell-cycle specific localization of the Rdi1p RhoGDI and the structural determinants required for Cdc42p membrane localization and clustering at sites of polarized growth. Curr Genet 2004;45:339–349. [PubMed: 15108020]

Rigler R, Foldes-Papp Z, Meyer-Almes FJ, Sammet C, Volcker M, Schnetz A. Fluorescence cross-correlation: a new concept for polymerase chain reaction. J Biotechnol 1998;63:97–109. [PubMed: 9772751]

Slaughter BD, Huff JM, Wiegraebe W, Schwartz JW, Li R. SAM domain-based protein oligomerization observed by live-cell fluorescence fluctuation spectroscopy. PLoS ONE 2008;3:e1931. [PubMed: 18431466]

Slaughter BD, Schwartz JW, Li R. Mapping dynamic protein interactions in MAP kinase signaling using live-cell fluorescence fluctuation spectroscopy and imaging. Proc Natl Acad Sci U S A 2007;104:20320–20325. [PubMed: 18077328]

Sopko R, Huang D, Smith JC, Figeys D, Andrews BJ. Activation of the Cdc42p GTPase by cyclin-dependent protein kinases in budding yeast. Embo J 2007;26:4487–4500. [PubMed: 17853895]

Spoerner M, Herrmann C, Vetter IR, Kalbitzer HR, Wittinghofer A. Dynamic properties of the Ras switch I region and its importance for binding to effectors. Proc Natl Acad Sci U S A 2001;98:4944–4949. [PubMed: 11320243]

Tiedje C, Sakwa I, Just U, Hofken T. The Rho GDI Rdi1 Regulates Rho GTPases by Distinct Mechanisms. Mol Biol Cell. 2008

Tkacz JS, Cybulska EB, Lampen JO. Specific staining of wall mannan in yeast cells with fluorescein-conjugated concanavalin A. J Bacteriol 1971;105:1–5. [PubMed: 5541005]

Tkacz JS, Lampen JO. Wall replication in saccharomyces species: use of fluorescein-conjugated concanavalin A to reveal the site of mannan insertion. J Gen Microbiol 1972;72:243–247. [PubMed: 4116719]

Wedlich-Soldner R, Altschuler S, Wu L, Li R. Spontaneous cell polarization through actomyosin-based delivery of the Cdc42 GTPase. Science 2003;299:1231–1235. [PubMed: 12560471]

Wedlich-Soldner R, Li R. Closing the loops: new insights into the role and regulation of actin during cell polarization. Exp Cell Res 2004;301:8–15. [PubMed: 15501439]

Wedlich-Soldner R, Wai SC, Schmidt T, Li R. Robust cell polarity is a dynamic state established by coupling transport and GTPase signaling. J Cell Biol 2004;166:889–900. [PubMed: 15353546]

Winter D, Podtelejnikov AV, Mann M, Li R. The complex containing actin-related proteins Arp2 and Arp3 is required for the motility and integrity of yeast actin patches. Curr Biol 1997;7:519–529. [PubMed: 9210376]

Zheng XD, Lee RT, Wang YM, Lin QS, Wang Y. Phosphorylation of Rga2, a Cdc42 GAP, by CDK/Hgc1 is crucial for Candida albicans hyphal growth. Embo J 2007;26:3760–3769. [PubMed: 17673907]

Ziman M, Preuss D, Mulholland J, O'Brien JM, Botstein D, Johnson DI. Subcellular localization of Cdc42p, a Saccharomyces cerevisiae GTP-binding protein involved in the control of cell polarity. Mol Biol Cell 1993;4:1307–1316. [PubMed: 8167411]

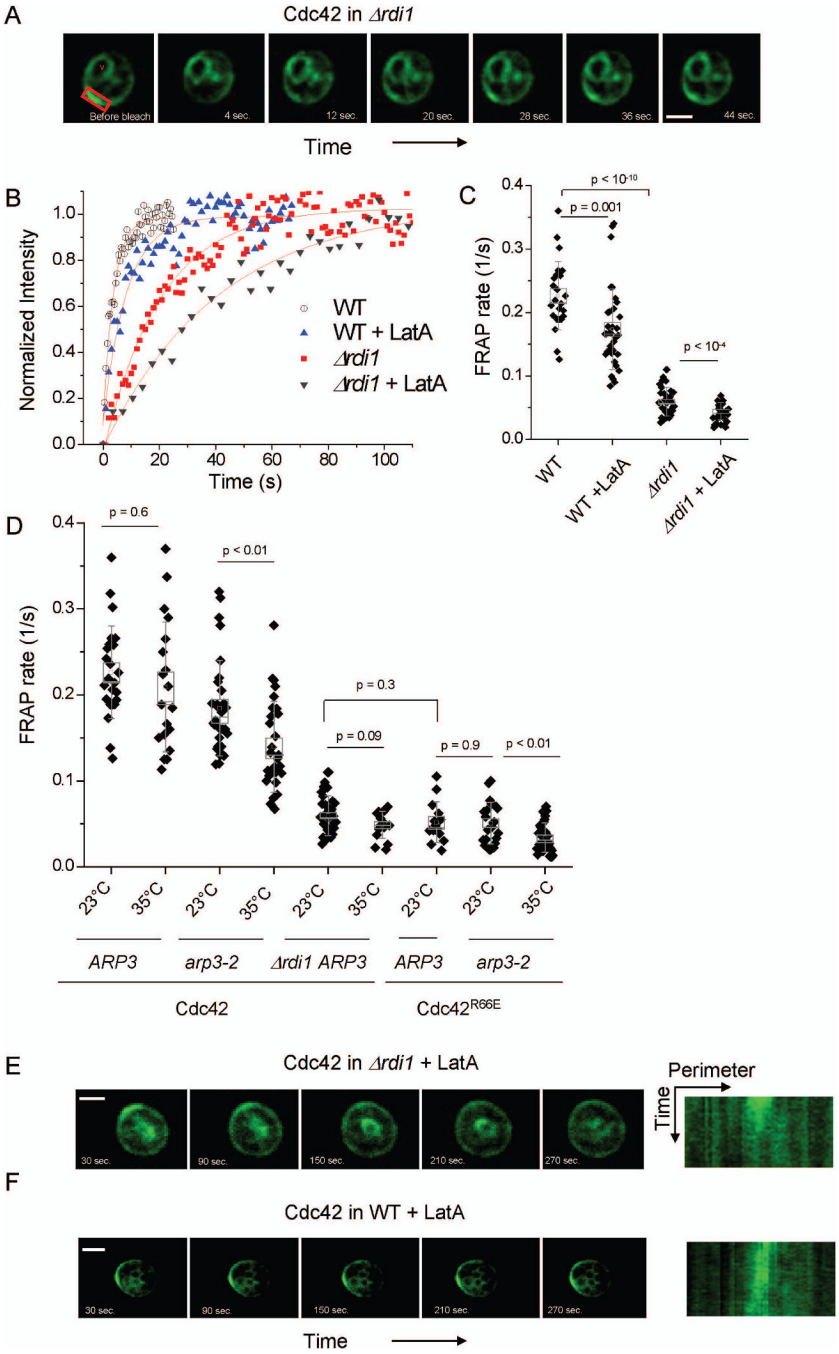

Figure 1. Cdc42 recycling examined with Fluorescence recovery after photobleaching (FRAP)

A. A montage of a FRAP analysis of a cell expressing GFP-Cdc42 in the *Δrdi1* background. The bleached region is marked in red, while a 'v' marks a vacuole. Scale bar is 2.0 μm. **B**. Normalized example curves for a subset of FRAP conditions. **C,D**. Rate of recovery (1/s) for FRAP measurements of GFP-Cdc42 under the conditions shown. Box width represents the standard error of the mean, whiskers represent the standard deviation. **E,F**. Montage and corresponding kymograph (fluorescence along perimeter of the cell) of Cdc42 in a *Δrdi1* and WT cell upon treatment with 100 μM LatA. Scale bar is 2.0 μm.

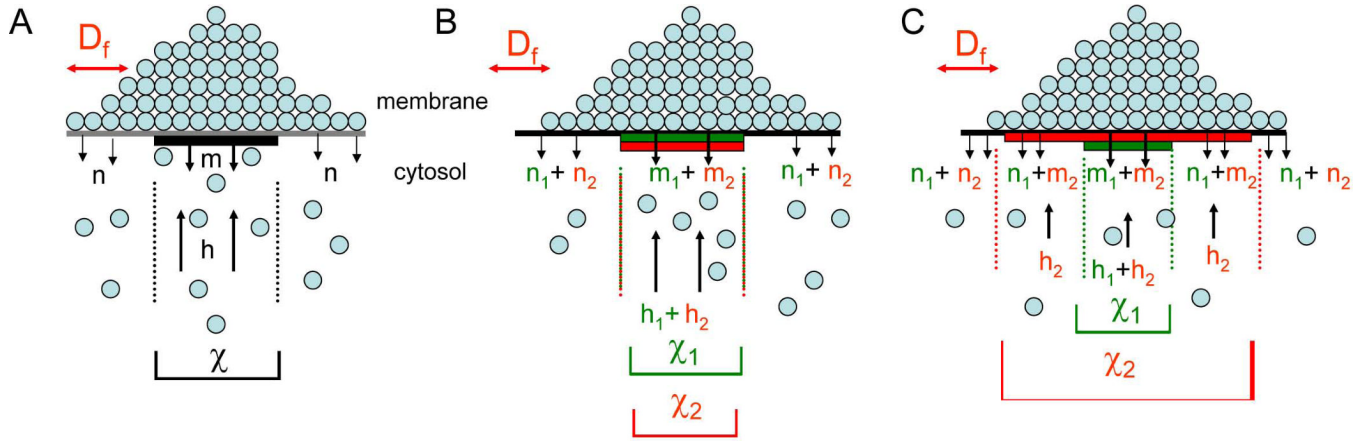

Figure 2. Modeling dynamic distribution of Cdc42 on the cortex

Basic depiction of the model, where D_f is the lateral diffusion in the membrane, *m* and *n* are the internalization rate inside and outside the delivery window, respectively. χ marks the delivery window, and *h* is the rate of delivery of molecules to the membrane (for more details, see Experimental procedures and Supplemental Information). (**A**) Shows the simplest scenario considering only one recycling pathway. (**B**) and (**C**) respectively show the model with overlapping Rdi1 and actin-based delivery windows of the same size or of different sizes (see Supplemental Information).

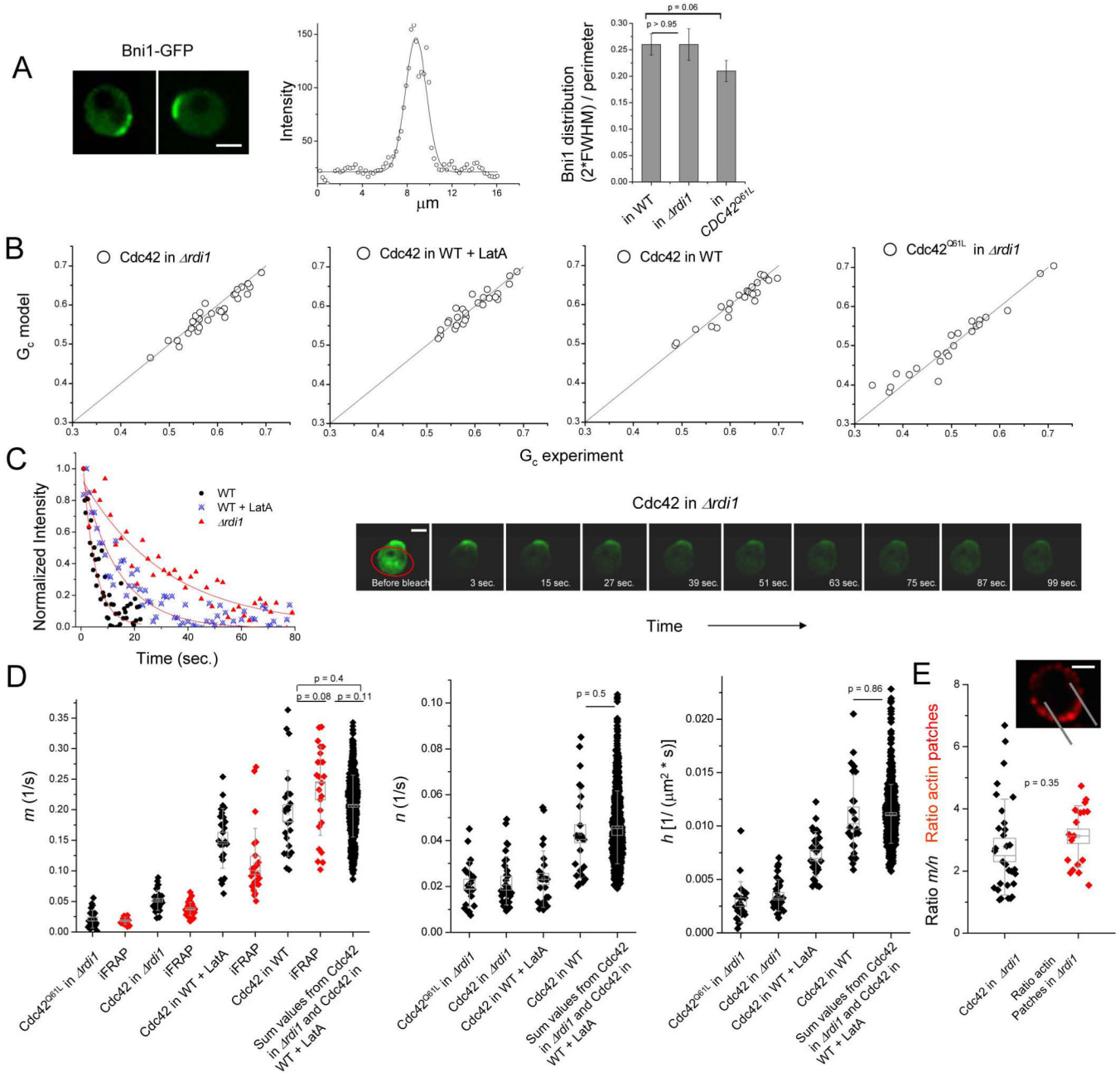

Figure 3. Determination of Cdc42 recycling parameters

A. The window of the actin-based recycling mechanism was estimated by the location of the formin, Bni1. Example images of Bni1-GFP are shown, along with an example fit of a perimeter trace to a Gaussian model. The window width is approximated as two times the full width half max (FWHM) of the Gaussian distribution. The average and standard error of the mean (SEM) of fits of n between 19 to 21 cells is shown. Bni1-GFP was used in WT and *Δrdi1* cells, while Bni1-mCherry was used in cells expressing GFP-Cdc42^{Q61L}. **B.** Relationship of G_c, or percentage of internal Cdc42 relative to total, as an output of the model relative to the experimental measurement. **C**. Example iFRAP curves, along with a montage of an example iFRAP measurement for a cell expressing GFP-Cdc42 in *Δrdi1*. Scale bar is 2.0 μm. The bleached region is circled in red. Fluorescence loss is measured in the cap. **D**. Output of model

parameters. Model calculated values of internalization rate inside the window (*m)* (in black) were compared to values measured experimentally by inverse FRAP (iFRAP) (in red). The values shown for the sum of the individual pathways represent all possible sums of all combinations. Box width represents SEM, whiskers represent the standard deviation (SD). **E**. Ratio of internalization rate inside the window to rate outside the window (*m/n)* from modeled parameters for the actin recycling pathway compared to the measured ratio of density of actin patches (using Arc40-mCherry) inside and outside the window defined by Bni1. Box width represents SEM, whiskers represent SD. An example of a summed time series for the actin patch marker Arc40-mCherry is shown, with the window marked (same cell as the left cell in **A**). Scale bar is 2.0 μm.

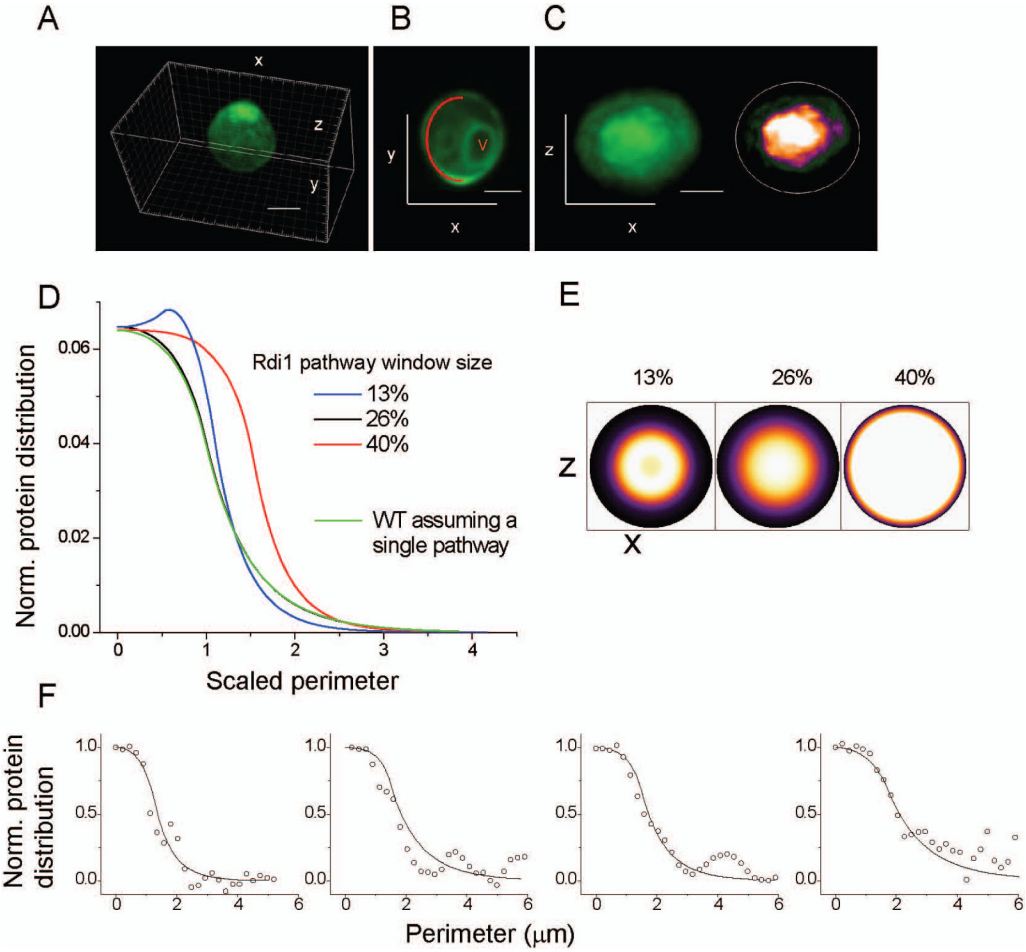

Figure 4. Effect of varying window size for Rdi1-dependent recycling on Cdc42 distribution

A-C. Example images depicting the orientations used for examination of the polar cap distribution. The red line in **B** represents the perimeter used as the x-axis in **D** and **E**. V marks a vacuole. **D,E**. Normalized output obtained by combining parameters for actin-based recycling with parameters for the Rdi1-pathway and using the dual pathway model (Fig. 2C). The actin pathway window size was held constant (26% perimeter) and Rdi pathway window sizes were varied as labeled. For comparison, the distribution obtained by modeling of Cdc42 in WT to a single pathway (window size: 26% perimeter) is shown. The y-axis represents the protein abundance in arbitrary units, while the x-axis represents the perimeter in scaled arbitrary units. **F.** Overlay of steady-state Cdc42 distributions observed experimentally in individual WT cells (dots) and those as calculated from model parameters extracted from imaging and FRAP data of the same cells (smooth line).

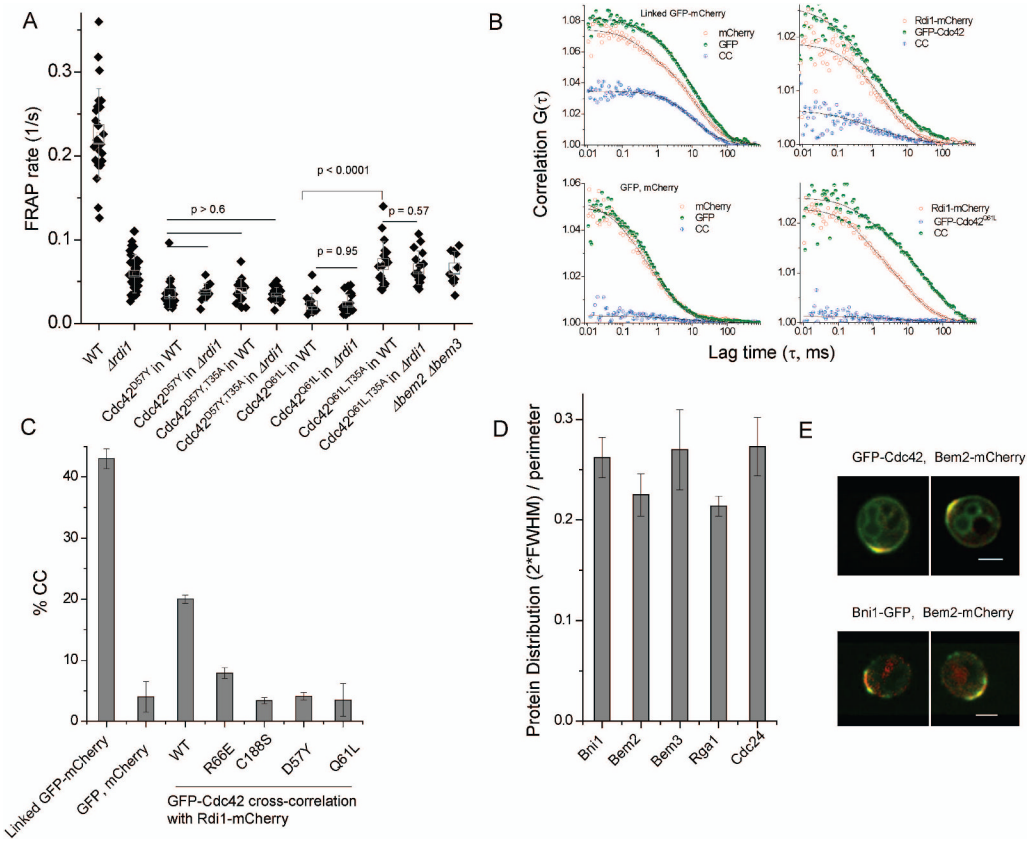

Figure 5. Effect of the GTPase cycle on Cdc42 recycling

A. FRAP rates (1/s) for conditions shown, Box width represents SEM, whiskers represent SD. **B**. Example fluorescence auto-correlation and cross-correlation curves in live yeast cells. Linked GFP and mCherry behind the cytosolic protein Bat2 (RLY2667) (Slaughter et al., 2007) or these fluorescent proteins expressed independently (RLY3291) were used as positive and negative controls, respectively. **C.** Quantification of cross-correlation between red and green species is shown as the percentage bound of the green (Cdc42) species (Slaughter et al., 2007). **D.** Width of the indicated protein distribution as a percentage of the perimeter, calculated as shown in Fig. 3. Error bars are the SEM (n = 8-22). **E.** Representative images to show overlap of the Bem2 distribution with the Cdc42 polar cap and with Bni1. Scale bar is 2.0 μm.

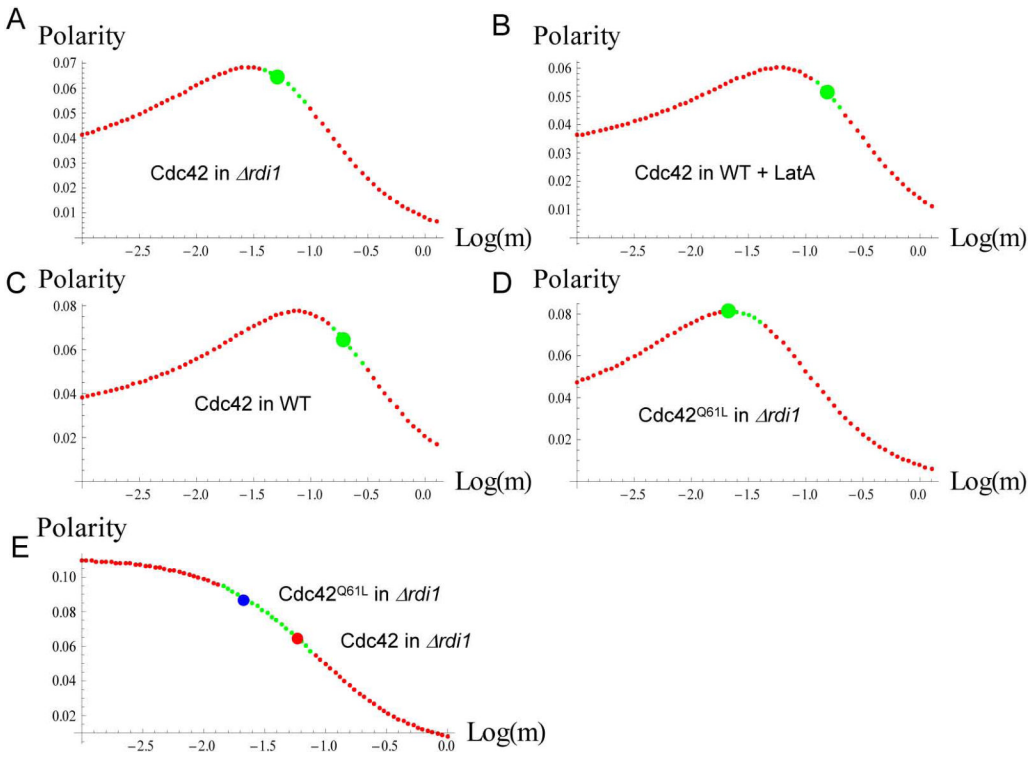

Figure 6. Polarity as a function of the internalization rate *m*

A-D. Polarity as the peak of the Cdc42 distribution divided by window width as a function of *m*, the rate of internalization inside the delivery window, for a *m/n* ratio fixed to the average value for each condition. "Allowed values" of G_c, (values that fit within the range observed experimentally), are shown in green. The large green point represents the value on the curve calculated from the measured *m* value for that condition. **E**. Polarity plotted as a function of *m* for a fixed value of *n*. As in (A), green dots represent the experimentally observed range of G_c.

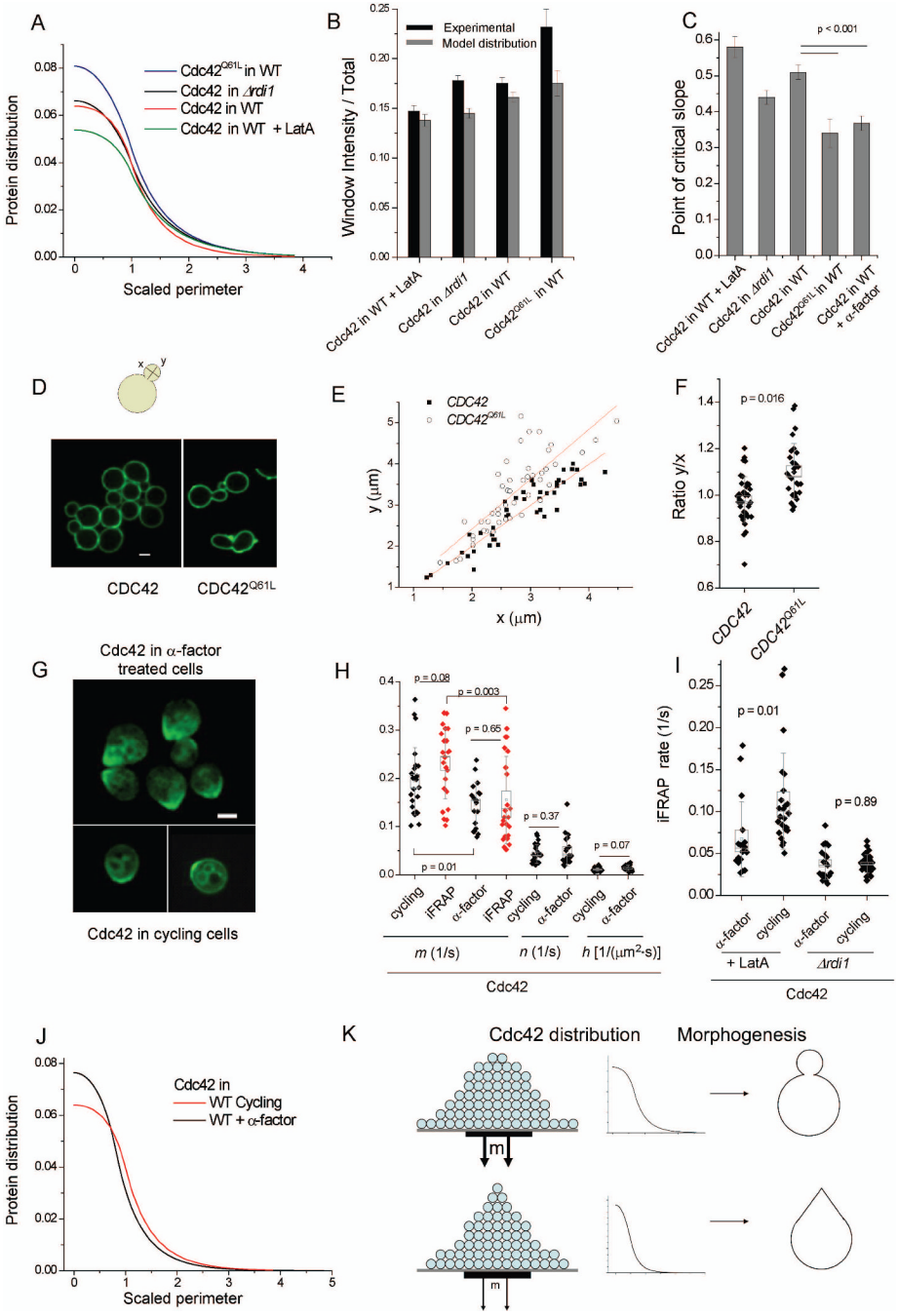

Figure 7. Effects of Cdc42 recycling on polarized morphogenesis

A. The steady-state Cdc42 distribution calculated from average *m*, *n*, and *h* values is shown for each condition. The y-axis represents the relative protein abundance in arbitrary units, while the x-axis represents the perimeter in scaled arbitrary units. Window size is scaled to 1.0 (See Supplemental Information). **B**. Relative intensity (arbitrary scale) of Cdc42 inside the window relative to total Cdc42 (membrane and internal), both from experimental measurements and the model-calculated steady-state distributions. **C**. The distance from the cap center at which a critical slope is reached (see main text) is shown. **D**. Cells labeled with FITC-Concanavalin-A to mark the cell wall. Representative images are shown. Scale bar is 2.0 μm. **E**. Plots of y vs. x in cells expressing Cdc42 or Cdc42^{Q61L} stained as described in (**D**). Each point represents

a measured cell. **F**. Quantification of y/x ratio for buds with width smaller than 3 μm. Box width represents SEM, whiskers represent SD. **G.** Cdc42 localization and characteristic pointed shape of WT cells after 1.5 hours of treatment with 75 μM α-factor, compared to cycling cells. Scale bar is 2.0 μm. **H**. Model parameters extracted from FRAP data and imaging (black), and internalization rate inside the window from independent iFRAP measurements (red) for comparison of Cdc42 in cycling cells (same as Fig. 3D) and in cells treated with α-factor. **I**. Internalization rates measured by iFRAP for cycling cells or cells after 1.5 hours of treatment with 75 μM α-factor either in the presence of 100 μM LatA or in the background of *Δrdi1*. **J.** Steady-state Cdc42 distributions calculated from average values from modeled data. Axes are as described in (A). **K**. Summary of the relationship of the recycling parameter *m* to the Cdc42 membrane-distribution and subsequent morphogenesis. Reduction in internalization rate inside the window (*m)* upon pheromone response leads to a pointed Cdc42 distribution, which in turn facilitates pointed growth to form a mating projection.